Transient Thermal Model for Radial Active Magnetic Bearing

Riku Pöllänen, Janne Nerg, Marko Rilla and Olli Pyrhönen
Department of Electrical Engineering
Lappeenranta University of Technology
P.O.Box 20, 53851 Lappeenranta, Finland
Riku.Pollanen@lut.fi

***Abstract*— A lumped-parameter thermal model capable of both static and transient analysis for a radial active magnetic bearing is presented. The determination of the electromagnetic state of the bearing using reluctance network method is proposed and the analytical calculation of four different power loss sources is discussed in details. The thermal model is tested by determing the power losses, steady state temperature distribution and transient temperature response of a prototype 8-pole magnetic bearing.**

***Index Terms*— Magnetic bearings, thermal modeling, power losses**

I. Introduction

In active magnetic bearings, the design of heat transfer is of equal importance as the electromagnetic design of the bearing, since the thermal rise of the bearing eventually decides the maximum current of the coils and thus the maximum force obtained from the bearing system. The heating of the bearing is due to the electromagnetic losses of the rotor and the stator cores and the ohmic losses of the stator windings. All of these loss components are strongly dependent on the operation point of the bearing, i.e. the angular velocity of the rotor and the current needed for the required force production. Furthermore, the eddy current losses of the rotor and the ohmic losses of the stator coils are temperature dependent via the temperature coefficient of the electrical resistivity. Besides the losses due to the bearing itself the fluid flowing in the air gap of the bearing is usually warmed by the losses of the electrical machine and the gas friction losses. This causes that the temperature of the cooling fluid could be considerably higher than the inlet temperature of the motor thus increasing the temperature at different parts of the bearing. The gas friction losses can be of significant importance especially when the bearing is operating at high speed. The rotating rotor gives a tangential velocity component for the air gap gas. In addition, the gas has also an axial velocity component if the cooling gas is blown through the air gap of the magnetic bearing. Both the tangential and axial velocities affect the friction torque of the bearing thus generating friction losses in the air gap. A comprehensive analysis on the friction losses of high-speed machinery is reported in [1].

Many researchers have developed thermal analysis methods for electrical machines. The most common approach is to utilize lumped parameters, i.e. thermal resistance networks as presented e.g. in [2] and [3]. Both of the studies were concentrated on the thermal analysis of an induction motor and both static and transient analysis was performed. [1] presented a static thermal model for high-speed induction motor where the heating of the cooling fluid was taken into account by utilizing a special cooling matrix. In this method, the cooling fluid flow inside the machine was modeled in terms of an additional matrix of thermal resistances. Because of the structural similarity between electric machines and radial active magnetic bearings, the same thermal analysis methods can be used in both applications. Examples of the lumped parameter based static thermal analysis of active magnetic bearing are given in [4] and [5]. However, in neither case the transient thermal analysis was considered.

In this paper a transient thermal analysis procedure for radial active magnetic bearing is presented. The cross-sectional geometry of the studied bearing is shown in Fig. 1. A two-dimensional reluctance network method (RNM) [6] is used to calculate the magnetic field distribution in the bearing geometry as well as the performance of the bearing, i.e. the coil current versus radial force characteristics, position and current stiffnesses and dynamic inductances of the coils. The rotational speed dependent eddy current and hysteresis losses of the rotor and the operating current dependent ohmic losses of the stator coils

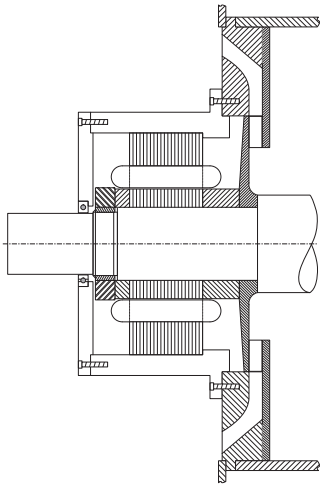

Fig. 1. Cross-sectional diagram of the modeled radial active magnetic bearing mounted on the end plate of a high speed electrical machine.

are evaluated using analytical equations. The modeling of the friction losses in the bearing air gap is also discussed. A thermal network model (TNM) exploiting the modeled loss components as thermal sources is used to calculate the temperature rise in different parts of the bearing. The temperature dependency of the TNM parameters is taken into account.

The model enables the determination of the bearing hot spots and the thermal current limitation in the coils at the selected ambient temperature. By combining the proposed TNM with the thermal model of the high speed electrical machine the operation temperatures and the cooling requirements in terms of the cooling gas mass flow rate meeting the specified temperature rises can be predicted.

II. MODELING

A. Reluctance network model

In the reluctance network model, Maxwell's field equations are reduced to a set of magnetic circuit equations. The magnetic circuit is composed of sources describing the magneto-motive forces created by the windings and reluctances representing different parts of the geometry. In order to keep the model complexity reasonable some simplifications and assumptions are made. The bearing geometry is modeled in Cartesian 2-D plane, i.e. the coil end effects are not taken into account. An uniform flux distribution in the flux path cross sections is assumed and that the leakage flux flows only in the modeled leakage paths. Due to the laminated rotor and stator cores the eddy currents and hysteresis are assumed to have negligible effects on the distribution of the air gap flux. With these assumptions the field equations and the material properties connecting the magnetic field intensity and the magnetic flux density can be combined into a relative small group of nonlinear algebraic equations. As a solution of these equations the magnetic field distribution is obtained.

Fig. 2a shows a geometry of the studied eight-pole radial active magnetic bearing. In Fig. 2b the equivalent reluctance network model with definitions of loop-fluxes Φ_i and branch fluxes ϕ_i is presented. The geometry is divided to reluctances representing the stator yoke $\Re_{sy}$, upper $\Re_{zup}$ and lower $\Re_{zlow}$ part of the stator tooth, stator slot $\Re_{slot}$, air gap $\Re_{\delta}$ and rotor yoke $\Re_{ry}$. Magneto-motive forces created by the coils are modeled with sources denoted by $N/2i_k$.

Initial values of the rectangular reluctances are calculated as

$$\Re_i = l_i/(\mu_i A_i) \tag{1}$$

where l_i is the length of the reluctance in the direction of the flux density, A_i is the cross sectional area of the reluctance and μ_i is the permeability of the unsaturated branch material. For arched reluctance the equation

$$\Re_i = \frac{\theta_i}{\mu_i z_i \ln\left(\frac{r_{\mathrm{out}}}{r_{\mathrm{in}}}\right)} \tag{2}$$

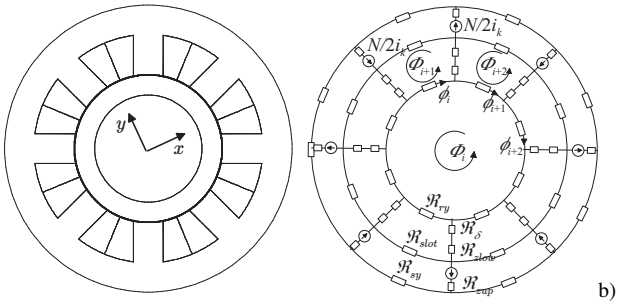

Fig. 2. Geometry a) and reluctance network model b) of radial AMB. N is the number of coil turns per pole pair, Φ_i and ϕ_i are the ith loop and branch fluxes, respectively.

where θ_i is the arc angle, z_i is the axial length of the branch and r_{out} and r_{in} are the outer and inner radius of the branch can also be considered. Between the iteration steps the reluctances consisting of nonlinear iron are updated using the formula

$$\Re_i(\phi_i) = H_i(B_i) l_i/\phi_i \tag{3}$$

where B_i is the branch flux density and the field intensity $H_i(B_i)$ is evaluated from the magnetization curve of the stator and rotor core material using the cubic spline interpolation.

The nonlinear equations of the RNM can be expressed in the matrix form as

$$\mathbf{T}\Re(\phi)\mathbf{T}^{\mathrm{T}}\mathbf{\Phi} = \mathbf{N}\mathbf{i} \tag{4}$$

where $\Re$ is the diagonal reluctance matrix, ϕ is the branch flux vector, $\mathbf{\Phi}$ is the loop-flux vector, $\mathbf{T}$ is the loop-set matrix connecting the branches to correct loops, $\mathbf{i}$ is the coil current vector and $\mathbf{N}$ is the matrix, which couples the coil currents to the magneto-motive force of the loops. Loop-fluxes are solved iteratively using the following Newton-Raphson algorithm

$$\mathbf{\Phi}^{k+1} = \mathbf{\Phi}^k - \left(\mathbf{T}\left[\mathbf{J}\Re(\phi)\phi\right]^k\mathbf{T}^{\mathrm{T}}\right)^{-1}\mathbf{r}^k \tag{5}$$

$$\mathbf{J}\Re(\phi)\phi = \partial(\Re(\phi)\phi)/\partial\phi \tag{6}$$

$$= \mathrm{diag}\left[\begin{array}{ccc} \frac{\partial\Re_i(\phi_i)\phi_i}{\partial\phi_i} & \cdots & \frac{\partial\Re_M(\phi_M)\phi_M}{\partial\phi_M}\end{array}\right]$$

$$\mathbf{r} = \mathbf{T}\Re(\phi)\mathbf{T}^{\mathrm{T}}\mathbf{\Phi} - \mathbf{N}\mathbf{i} \tag{7}$$

where $\mathbf{J}$ is the Jacobian matrix, $\mathbf{r}^k$ is the residual of the kth iteration step and M is the total number of the branch fluxes.

B. Losses

1) Eddy current losses: Eddy current power losses in the laminated rotor are evaluated by using the analytical method presented in [7]. However, instead of using the proposed analytical field solutions for both the lamination and the air gap, we exploit the numerical solution obtained from the RNM. The total eddy current loss of the rotor

is obtained as a sum of the power loss contributions from each air gap flux harmonic

$$P_{\mathrm{e}} = ULau^{3/2}\sqrt{\frac{\sigma}{\mu}}\sum_{n=1}^{\infty}\left[\eta\coth\left(k_n W_{\mathrm{r}}\right)\frac{\sqrt{k_n}C_n^2}{\gamma^2}\right] \quad (8)$$

where U is the circumference at the tip of the pole of the stator, L is the axial length of the journal, a is the lamination thickness, u is the peripheral speed of the rotor, W_{r} is the radial width of the rotor lamination and σ and μ are the conductivity and permeability of the rotor lamination material. Parameter γ and the rotating effect number η are defined by

$$\gamma = \cosh\left(k_n\delta\right) + \frac{1}{\mu_{\mathrm{r}}}\coth\left(k_n W_{\mathrm{r}}\right)\sinh\left(k_n\delta\right) \quad (9)$$

$$\eta = \frac{\sinh\sqrt{nRe_{\mathrm{m}}} - \sin\sqrt{nRe_{\mathrm{m}}}}{\cosh\sqrt{nRe_{\mathrm{m}}} - \cos\sqrt{nRe_{\mathrm{m}}}} \quad (10)$$

where δ is the radial air gap length, μ_r is the relative permeability of the rotor material. Re_{m} is the magnetic Reynolds number defined as

$$Re_{\mathrm{m}} = \frac{a^2\omega\mu\sigma}{4} \quad (11)$$

where ω is the angular velocity of the rotor and n is the order of the harmonic. Coefficients C_n are obtained from the Fourier series approximation of the flux density $B(x)$ at the bearing pole surface

$$B(x) = \sum_{n=-\infty}^{\infty} C_n e^{ik_n x} \quad (12)$$

where $k_n = 2\pi n/U$ and x is the coordinate along the pole tip circumference.

2) Hysteresis and ohmic losses: Hysteresis losses are assumed to occur only in the rotor and they are modelled using the well-known equation of Steinmetz

$$P_{\mathrm{h}} = k_{\mathrm{h}} f \hat{B}^{1.6} V \quad (13)$$

where k_{h} is the hysteresis loss coefficient of the rotor material, f is the frequency of the cyclic magnetization, $\hat{B}$ is the peak flux density in the iron and V is the volume of the iron. For the paired pole configuration the magnetization frequency is twice the rotor rotation frequency.

Total ohmic loss taking place in the stator coils is calculated as

$$P_{\mathrm{cu}} = \sum_{i=1}^{8} R_{\mathrm{coil},i}(T_i) I_{\mathrm{coil},i}^2 \quad (14)$$

where $I_{\mathrm{coil},i}$ is the current and $R_{\mathrm{coil},i}(T_i)$ is the resistance of the ith coil at the temperature T_i. The temperature dependency of the coil resistance is taken into account by

$$R_{\mathrm{coil},i}(T_i) = \left[1 + \alpha_{\mathrm{cu}}\left(T_i - T_\infty\right)\right] R_{\mathrm{coil},i}(T_\infty) \quad (15)$$

where α_{cu} is the temperature coefficient of the resistivity of copper and T_∞ is the ambient temperature.

3) Friction losses: Losses due to the gas friction affect indirectly to the temperature rise of the bearing because the friction losses heat the cooling fluid. The friction losses in the air gap of the bearing can be estimated by the equations derived for rotating cylinders in enclosures. The friction power P_{fr} associated with the resisting drag torque of a rotating cylinder can be written as [1]

$$P_{\mathrm{fr}} = k_1 C_{\mathrm{T}} \rho\pi\omega^3 r^4 l \quad (16)$$

where C_{T} is the torque coefficient, ρ is the mass density of the cooling fluid, ω is the angular velocity, r is the radius and l is the length of the cylinder. k_1 is the roughness coefficient the value of which is 1.0 for smooth surfaces and typically $2\ldots4$ for slotted surfaces.

When a rotor is rotating in enclosure, i.e. inside the stator, the nature of the tangential cooling gas flow exerted by the rotating cylinder can be determined using the Couette Reynolds number, defined as

$$Re_\delta = \frac{\rho u\delta}{\mu_{\mathrm{cf}}} \quad (17)$$

where μ_{cf} is the dynamic viscosity of the cooling fluid. According to the measurements reported in [8] the torque coefficients equations within the different flow regimes are

$$C_{\mathrm{T}} = 0.515\frac{\left(\frac{\delta}{r}\right)^{0.3}}{Re_\delta^{0.5}} \quad \left(500 < Re_\delta < 10^4\right) \quad (18)$$

$$C_{\mathrm{T}} = 0.0325\frac{\left(\frac{\delta}{r}\right)^{0.3}}{Re_\delta^{0.2}} \quad \left(Re_\delta > 10^4\right) \quad (19)$$

The friction losses increase if there is an axial gas flow through the air gap of the bearing. The rotor forces the cooling gas into a tangential movement and some power is needed for this acceleration. If the radial air gap length is small compared to the rotor radius, the power loss due to axial flow can be approximated with

$$P_{\mathrm{fr,a}} = k_2 q_{\mathrm{m}} u^2 \quad (20)$$

where k_2 is the velocity factor and q_{m} is the mass flow rate of the cooling gas. The velocity factor depends on whether the flow is laminar or turbulent and the roughness of the air gap surfaces. According to [9], the theoretical velocity factor gets a value of 0.48 in turbulent flow. However, the real value for the velocity factor can be expected to be much lower. According to the results reported in [10], the velocity factor, in case of a smooth rotor surface, gets a value of 0.18 for a smooth stator surface and 0.15 for a rough, i.e. slotted stator surface. Thereby, the stator slotting decreases the losses associated with the axial cooling gas flow through the air gap. It must be noticed that the mass flow rate dependent friction loss turns into heat after the air gap, i.e. it does not affect to the radial heat transfer of the rotor and the stator cores of the bearing.

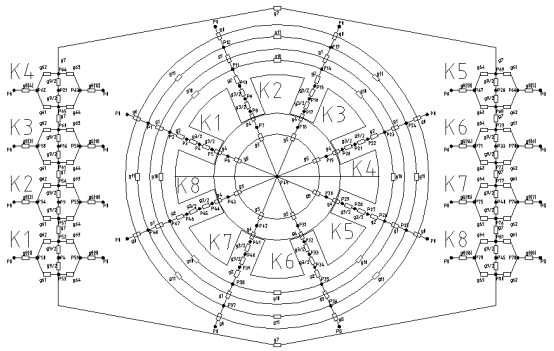

Fig. 3. Thermal network model of the radial active magnetic bearing.

C. Thermal network model

In the thermal network model the geometry of the studied radial active magnetic bearing is divided into 6 parts, i.e. rotor, stator core, upper and lower part of the stator teeth, air-gap and stator winding. The developed thermal resistance network presented in Fig. 3 consists of 81 nodes and 120 thermal resistances. All heat transfer mechanisms, i.e. thermal conduction, convection and radiation as well as the effect of the temperature on the thermal material properties of the bearing and the cooling fluid are taken into account in the model. Due to laminated structure of the stator and rotor the axial heat conduction is assumed to be negligible except in the coils and shaft.

The general equation for the thermal resistance describing the heat conduction is

$$R_{\mathrm{cond}} = \frac{L}{\lambda A} \tag{21}$$

where L is the length of the heat transfer path, λ is the thermal conductivity and A is the cross-sectional area of the surface normal to the direction of the heat transfer. The convection heat transfer between solid surfaces and cooling gas is modeled using a single thermal resistance R_{conv} defined as

$$R_{\mathrm{conv}} = \frac{1}{\alpha A} \tag{22}$$

where α is the convection coefficient. The thermal contact resistances due to the contact transitions, e.g. between the stator and the frame, are modeled in a similar manner by substituting the convection coefficient with the contact heat transfer coefficient. The thermal radiation between solid surfaces i and j is modeled as a single thermal resistance R^{ij}_{rad} defined as

$$R^{ij}_{\mathrm{rad}} = \frac{T_i - T_j}{\epsilon \sigma_{\mathrm{SB}} \left(T_i^4 - T_j^4\right) F_{ij} A_i} \tag{23}$$

where T_i and T_j are the absolute temperatures of the surfaces, respectively, ϵ is the emissivity, σ_{SB} is the Stefan-Boltzmann's constant, F_{ij} is the view factor between surfaces and A_i is the area of the radiating surface.

The most important convection coefficients to be evaluated are the convection coefficients between the stator and the air gap as well as between the rotating rotor and the air gap. The air gap flow can be considered as a channel flow and its Nusselt number is given by

$$Nu = \frac{\alpha \delta}{\lambda} \tag{24}$$

where λ is now the thermal conductivity of the cooling fluid. The correlation equations for the Nusselt number is found as a function of the Taylor number defined as

$$Ta = \frac{\rho^2 \omega^2 r_\delta \delta^3}{\mu^2_{\mathrm{cf}}} \tag{25}$$

where r_δ is the mean radius of the air gap. Regarding the value of the Taylor number the Nusselt number is [11]

$$Nu = 2 \quad (Ta < 1740) \tag{26}$$

$$Nu = 0.409 Ta^{0.241} - 137 Ta^{-0.75} \quad (Ta \geq 1740) \tag{27}$$

The other convection coefficients were evaluated using the correlation equations found e.g. in [12].

For steady-state analysis, the temperature rise of the each node of the thermal network relative to the reference temperature is calculated using the matrix equation

$$\Delta \mathbf{T} = \mathbf{G}^{-1} \mathbf{P} \tag{28}$$

where $\mathbf{P}$ is the power loss vector containing the losses at each node and $\Delta \mathbf{T}$ is the temperature rise vector. In the developed thermal model the thermal resistances of different parts of the bearing are used to generate an 81×81 thermal conductance matrix $\mathbf{G}$ defined as

$$\mathbf{G} = \begin{bmatrix} \sum_{i=1}^{81} \frac{1}{R_{1,i}} & -\frac{1}{R_{1,2}} & \cdots & -\frac{1}{R_{1,81}} \\ -\frac{1}{R_{2,1}} & \sum_{i=1}^{81} \frac{1}{R_{2,i}} & \cdots & -\frac{1}{R_{2,81}} \\ \vdots & \vdots & \ddots & \vdots \\ -\frac{1}{R_{81,1}} & -\frac{1}{R_{81,2}} & \cdots & \sum_{i=1}^{81} \frac{1}{R_{81,i}} \end{bmatrix} \tag{29}$$

where the nth diagonal element is the sum of the network conductances connected to node n, and $G(i,j)$ is the thermal conductance connecting the nodes i and j.

In transient problems, a representation for the stored thermal energy in the system is introduced as thermal capacitances. Each node is assigned with a thermal capacitance from the node to the ambient. The thermal capacitance of such an element is calculated as

$$C_{\mathrm{th},i} = \sum_{j=1}^{n} m_j c_{\mathrm{p},j} \tag{30}$$

where m is the mass, c_{p} is the heat capacity and index j signifies different materials in the same element. By defining a thermal capacitance matrix

$$\mathbf{C} = \begin{bmatrix} C_{\mathrm{th},1} & 0 & \cdots & 0 \\ 0 & C_{\mathrm{th},2} & \cdots & 0 \\ \vdots & \vdots & \ddots & \vdots \\ 0 & 0 & \cdots & C_{\mathrm{th},81} \end{bmatrix} \tag{31}$$

the derivatives of the temperature rises relative to a reference temperature are found by solving

$$\frac{d}{dt}\left(\Delta\mathbf{T}\right) = \mathbf{C}^{-1}\left(\mathbf{P} - \mathbf{G}\Delta\mathbf{T}\right) \tag{32}$$

Final temperature rises are numerically integrated using Heun's method with a fixed time step of 0.25 s.

III. Calculation Procedure

The calculation procedure of the model is divided into modular steps as indicated in the flowchart shown in Fig. 4. In the first step the bearing geometry and initial material properties are read into memory. The second step includes the calculation of the magneto-motive forces and initial branch reluctances for the RNM and thermal resistances and capacitances for the TNM. Operation point variables introduced at this point consist of the four coil currents $I_{\mathrm{coil},i}$, $i = 1...4$, ambient temperature T_∞, which represents also the temperature of the cooling fluid, and the rotational speed of the rotor ω. After this the magnetic field distribution in the bearing is solved using the RNM and the air gap flux density $B(x)$ is delivered to loss calculation block. In RNM a centered rotor is assumed although the model is also able to handle the eccentric situations.

Next the iteration or time step loop comprising the calculation of power loss components and temperature increments or their derivatives is performed. In static problem the convergence criteria is tested after each iteration step. If the solution has not converged the temperature dependent material properties and model parameters are updated and next iteration step is taken. If the convergence is reached or if we are solving the transient problem, the problem type and the end time criterion are checked. In case of the static model or if the final time of the transient simulation has been encountered, the final results are plotted and saved for the further analysis. Otherwise, the node temperatures and temperature dependent parameters are updated and the calculation of the next time step is started.

IV. Results

Developed thermal model was tested in the calculation of power losses as well as the static and transient temperature responses of an 8-pole radial active magnetic bearing designed and manufactured in Lappeenranta University of Technology. The dimensions and material parameters of the test bearing are in Table I. In all calculations the ambient and the average cooling air temperature of 20°C was assumed.

Fig. 5 presents the eddy current, hysteresis, friction, ohmic and total losses as a function of the rotational speed. The bearing coil currents were 3.75 A. At the nominal rotational speed of the machine (12000 rpm) the eddy current losses and the total losses are estimated to be 21 W and 61 W, respectively. Ohmic losses show an interesting behavior. They seem to first somewhat decrease when the rotational speed is increased. This can be explained by the fact that the coil resistances decrease due to improved cooling by the convection when the speed increases. The

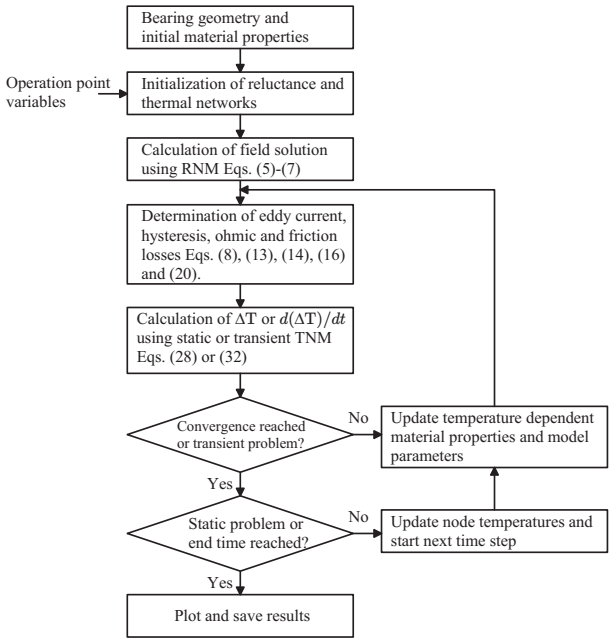

Fig. 4. Simplified flowchart of the calculation procedure.

TABLE I

Dimensions and magnetic material parameters of the test bearing

Stator outer diameter	180 mm	Relative permeability	7000
Core length	60 mm	Electrical resistivity	0.55 $\mu\Omega$m
Shaft diameter	60 mm	Thermal conductivity	52 $\frac{\mathrm{W}}{\mathrm{mK}}$
Rotor outer diameter	89.8 mm	Hysteresis loss coefficient	200 $\frac{\mathrm{J}}{\mathrm{m}^3}$
Air gap	0.6 mm	Static air gap flux density	0.7 T
Pole width	18 mm	Coil resistance	0.58 Ω
Lamination thickness	0.5 mm	Number of turns per pole	90

same can be observed also in Fig. 6 where the steady state temperatures of the selected nodes at different rotational speeds are shown. After a certain point, however, the power losses in the rotor compensate this effect and the coil temperatures and the ohmic losses start increase again. Rotor temperature increases continuously as a function of the rotational speed due to increasing eddy current and friction losses. Generally, the nodal temperatures at the investigated speed range are within an acceptable level.

Typically, the bias current is chosen to be half of the maximum bearing current yielding an equally large current amplitude available for control. This selection leads to extensive power losses in totally and the maximum operational temperature of the windings may be exceeded. The proposed calcucation model can be also utilized in selecting an appropriate bias current as a trade off between sufficient control performance and bearing temperatures. An example is given in Fig. 7 where the effect of the bias current level on the node temperatures at 12000 rpm is presented. It is seen that by reducing the bias current from 5 A to 3.75 A the coil temperature is approximately halved.

Finally Fig. 8 shows the temperature transient due to start up at 6000 rpm and a rotational speed step from 6000 rpm to 12000 rpm. From the responses it is observed that

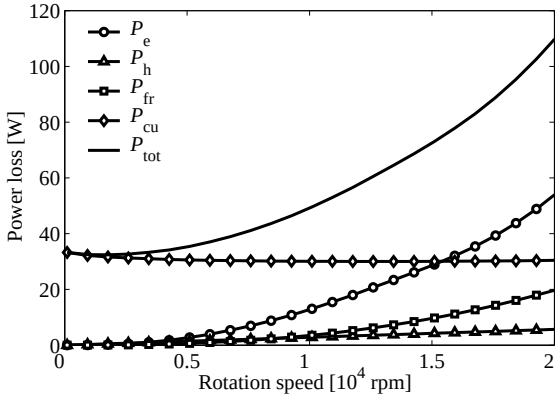

Fig. 5. Calculated power losses. $I_{\mathrm{coil},i} = 3.75A$.

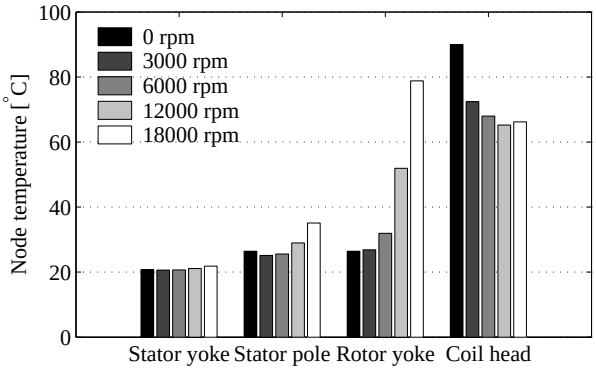

Fig. 6. Temperatures of selected nodes at different rotational speeds. $I_{\mathrm{coil},i} = 3.75A$.

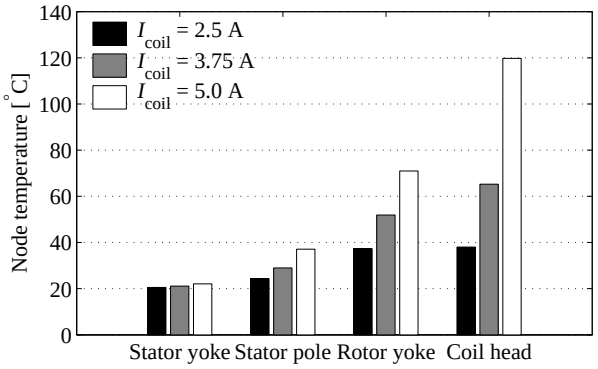

Fig. 7. Comparison of the node temperatures at different coil currents. $\omega = 12000$ rpm.

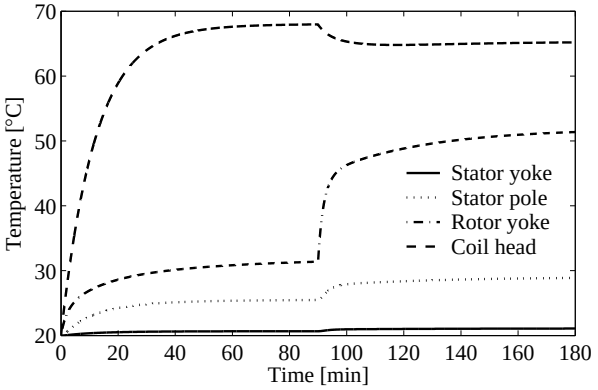

Fig. 8. Transient temperature responses due to start up at 6000 rpm and a rotational speed step from 6000 rpm to 12000 rpm. $I_{\mathrm{coil},i} = 3.75A$.

the temperatures converge accurately to steady state values predicted in Fig. 6. At rotational speed of 6000 rpm the average settling times of the coil and rotor temperatures are about 45 and 90 min, respectively.

V. Conclusions

Static and transient thermal model of radial active magnetic bearing was presented. Magnetic conditions of the bearing were solved using the reluctance network model and the different power loss components were evaluated from analytical expressions. Temperature dependency of the material properties was taken into account. The developed thermal model can be used to determine the power losses and temperature distribution of the bearing in steady state conditions as well as in the transition between different operation points. Future work will include the final tuning of the model parameters and the experimental verification of the calculated results.

References

[1] J. Saari, "Thermal analysis of high-speed induction machines," Acta Polytechnica Scandinavia, Electrical Engineering Series no. 90, Diss. HUT, Espoo, Finland, 1998.

[2] P. D. Mellor, D. Roberts, D. R. Turner, "Lumped parameter thermal model for electrical machines of TEFC design," IEE Proceedings-B, vol. 138, no. 5, pp. 205-218, September 1991.

[3] G. Kylander, "Thermal modeling of small cage-induction motors," Ph. D. thesis, Chalmers University of Technology, Gothenburg, Sweden, 1995.

[4] A. Traxler, "Eigenschaften und Auslegung von berührungsfreien elektromagnetischen Lagern," Diss., ETH Zurich, 1985.

[5] L. Burdet, B. Aeschlimann, R. Siegwart, "Thermal model for a high temperature active magnetic bearing," Proceedings of the Ninth International Symposium on Magnetic Bearings (ISMB9), Kentucky, August 3-6, 2004.

[6] J. Nerg, R.Pöllänen, J. Pyrhönen, "Modeling the force versus current characteristics, linearized parameters and dynamic inductance of radial active magnetic bearings using different numerical calculation methods," WSEAS Trans. Circuits and Systems, vol. 4, no. 6, pp. 551-559, June 2005.

[7] S. Yanhua, Y. Lie, "Analytical method for eddy current losses in laminated rotors with magnetic bearings," IEEE Trans. Magnetics, vol. 38, no. 2, pp. 1341-1347, March 2002.

[8] E. Bilgen, R. Boulos, "Functional dependence of torque coefficient of coaxial cylinders on gap width and Reynolds numbers," Transactions of ASME, Journal of Fluids Engineering, series I, vol. 95, pp. 122-126, 1973.

[9] J. W. Polkowski, "Turbulent flow between coaxial cylinders with inner cylinder rotating," Transactions of ASME, Journal of Engineering for Gas Turbines and Power, vol. 106, no. 1, pp. 128-135, 1984.

[10] F. Kreith, "Convection heat transfer in rotating systems," Advances in Heat Transfer, vol. 5, Academic Press Inc., pp. 129-246, 1968.

[11] K. M. Becker, J. Kaye, "Measurements of diabatic flow in an annulus with an inner rotating cylinder," Transactions of ASME, Journal of Heat Transfer, vol. 84, pp. 97-105, May 1962.

[12] F. D. Incropera, D. P. DeWitt, "Fundamentals of mass and heat transfer," 2nd edition, John Wiley & Sons, Singapore, 1985.